

On the Segmentation of 3D LIDAR Point Clouds

B. Douillard, J. Underwood, N. Kuntz, V. Vlaskine, A. Quadros, P. Morton, A. Frenkel
The Australian Centre for Field Robotics, The University of Sydney, Australia

Abstract—This paper presents a set of segmentation methods for various types of 3D point clouds. Segmentation of dense 3D data (e.g. Riegl scans) is optimised via a simple yet efficient voxelisation of the space. Prior ground extraction is empirically shown to significantly improve segmentation performance. Segmentation of sparse 3D data (e.g. Velodyne scans) is addressed using ground models of non-constant resolution either providing a continuous probabilistic surface or a terrain mesh built from the structure of a range image, both representations providing close to real-time performance. All the algorithms are tested on several hand labeled data sets using two novel metrics for segmentation evaluation.

I. INTRODUCTION

This paper presents a set of segmentation methods for 3D LIDAR data. Segmentation is a critical pre-processing step in a number of autonomous perception tasks. It was for example recently shown by Malisiewicz and Efros [7] that prior segmentation improves classification in computer vision applications. The aim of this study is to provide a set of segmentation techniques tailored to different types of 3D data (Fig. 1 and 3(c)) that can be integrated to larger processing pipelines such as classification, dynamic object tracking and path planning.

We anticipate 3D sensing to be pivotal in the development of artificial perception. Recent 3D sensor developments (e.g. Velodyne, Riegl, Ibeo) lead to increased perceptual ability, complementing vision data by addressing illumination variation from monocular imagery and sparse reconstruction of geometry from stereo. The associated high data rate requires quality conditioning, which can be obtained from segmentation techniques.

II. RELATED WORK

Segmentation has been studied for several decades and in particular in computer vision where it is often formulated as graph clustering. Instances of such approaches are Graph Cuts [2] including Normalised Cuts [14] and Min Cuts [18]. Graph-cuts segmentation has been extended to 3D point clouds by Golovinskiy and Funkhouser [5] using k-nearest neighbours (KNN) to build a 3D graph and assigning edge weights according to an exponential decay in length. The method requires prior knowledge on the location of the objects to be segmented.

The recent segmentation algorithm of Felzenszwalb and Huttenlocher (FH) [10] for natural images has gained popularity for robotic applications due to its efficiency [13], [15], [16], [19]. Zhu *et al.* build a 3D graph with KNN while assuming the ground to be flat for removal during pre-processing. 3D partitioning is then obtained with the FH

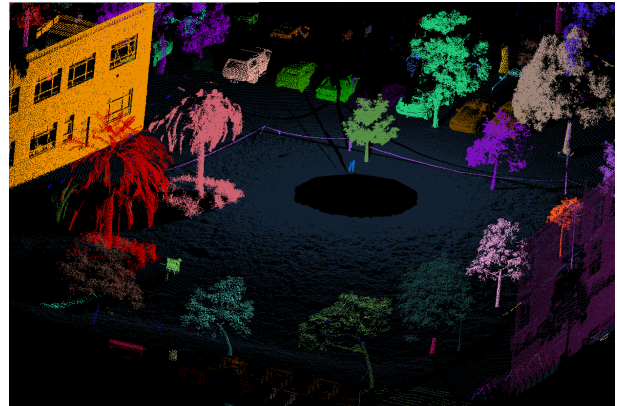


Fig. 1. An example of segmentation obtained with the Cluster-All (Sec. III-B.2) method applied to one of the test dense data sets. Colours are mapped to segments IDs. This segmentation corresponds to a point score of 97.4 and a voxel score of 94.3 (point and voxel scores are defined in Sec. IV).

algorithm [19]. Under-segmentation is corrected via posterior classification including the class “under-segmented”. Triebel *et al.* explore unsupervised probabilistic segmentation [16] in which the FH algorithm [10] is modified for range images and provides an over-segmentation during pre-processing. Segmentation is cast into a probabilistic inference process in two graphs modeled as Conditional Random Fields: one graph is used to segment in the range space and another graph is used to segment in feature space (built from 3D features such as Spin Images). The evaluation does not involve ground truth data. Schoenberg *et al.* [13] and Strom *et al.* [15] have applied the FH algorithm to coloured 3D data obtained from a co-registered camera laser pair. The former up-sample range data using the technique in [3] to obtain a depth value for each image pixel. The weights on the image graph are computed as a weighted combination of Euclidean distances, pixel intensity differences and angles between surface normals estimated at each 3D point. The FH algorithm is run on the image graph to provide the final 3D partitioning. The evaluation is done on road segments only, while the evaluation proposed here is performed on entirely hand labeled scans. Strom *et al.* propose a similar approach in which the FH algorithm is modified to integrate angle differences between surface normals in addition to differences in colour values. It is applied to a 3D graph built from a laser scan in which longer edges are disregarded. Segmentation evaluation is done visually without ground truth data.

A maximum spanning tree approach to the segmentation of 3D point clouds is proposed in [11]. Graph nodes represent Gaussian ellipsoids playing the role of geometric primitives.

The merging of ellipsoids during the growing of the tree is based on one of the two distance metrics proposed by the authors, each producing a different segmentation “style”. The resulting segmentation is similar to a super voxel type of partitioning (by analogy to super pixels in vision) with voxels of ellipsoidal shapes and various sizes.

Various methods focus on explicitly modeling the notion of surface discontinuity. Melkumyan defines discontinuities based on acute angles and longer links in a 3D mesh built from range data [8]. Moosman *et al.* use the notion of convexity in a terrain mesh as a separator between objects [9]. The latter approach is compared to the proposed algorithms in Sec. V-B.

The contribution of this work is multi-fold: a set of segmentation algorithms are proposed for various data densities, which neither assume the ground to be flat nor require a prior knowledge of the location of the objects to be segmented. The ground is explicitly identified using various techniques depending on the data type and used as a separator. Some of the proposed techniques are close to real-time and capable of processing any source of 3D data (Sec. III-C.1) or are optimised by exploiting the structure of the scanning pattern (Sec. III-C.2). All the methods are evaluated on hand labeled data using two novel metrics for segmentation comparison (Sec. V).

III. SEGMENTATION ALGORITHMS

A. Framework

This study considers the following three aspects of the segmentation problem. First, it investigates various types of 3D data: from dense (3D scans from a Riegl sensor for instance) to sparse (single Velodyne scans). Second, different types of model are used to represent and segment the ground. Three main types of ground models are explored: grid based (as in standard elevation maps [1], Sec. III-B), Gaussian Process based (Sec. III-C.1) and mesh based (Sec. III-C.2). Third, several types of 3D clustering techniques are tested and in particular 3D grid based segmentation with various cluster connectivity criteria is evaluated. The resulting algorithms are compositions of a ground model and a 3D clustering method. This study evaluates which algorithm provides better segmentation performance for each data type.

The notions of dense and sparse data are here defined based on a discretisation of the world with a constant resolution. A data set will be considered to be dense if the connectivity of most scanned surfaces can be captured with the connectivity of non-empty cells (cells receiving at least one data point). With sparser data, the number of empty cells increases which causes objects to be over-segmented. The algorithms proposed to segment dense data involve constant resolution grid-based models, while the algorithms proposed to process sparse data use ground representations which are of non-constant granularity and implement various types of interpolation mechanism as a way to bridge the holes in the data.

B. Segmentation for Dense Data

The general approach used for dense data is a voxel grid based segmentation. A three dimensional cubic voxel grid

is populated with 3D points and features are computed in each voxel. Features include 3D means and variances as well as density. This voxel grid approach is chosen due to its simplicity, ease of representation both visually and in data structures, and its ability to be scaled by adjusting voxel size to insure usable density of data in the voxels.

For dense data segmentation four different variations on this method are used, three of which have two stages and one which is single stage. The extra stage in the two stage processes is the determination of the ground partition, the common stage is a 3D clustering process. For all methods, voxels must meet minimum density requirements to be considered for segmentation.

1) *Ground Segmentation*: The ground partition is found by clustering together adjacent voxels based on vertical means and variances. If the difference between means is less than a given threshold, and the difference between variances is less than a separate threshold, the voxels are grouped. The largest partition found by this method is chosen as the ground.

2) *Cluster-All Method*: Ground segmentation is performed and the remaining non-ground points are partitioned by local voxel adjacency only. The size of the local neighbourhood is the only parameter. The ground is therefore operating as a separator between the partitions. The general outline of this method is shown in Algorithm 1. An example of segmentation it produces is shown in Fig. 1.

Input	: <i>pCloud</i>
Output	: <i>ground, voxelclusters</i>
Parameters	: <i>res, method</i>
1	<i>voxelgrid</i> \leftarrow FillVoxelGrid(<i>pCloud</i> , <i>res</i>) ;
2	<i>ground</i> \leftarrow ExtractGround(<i>voxelgrid</i>) ;
3	<i>voxelgrid</i> \leftarrow ResetVoxels(<i>voxelgrid</i> , <i>ground</i>) ;
4	<i>voxelclusters</i> \leftarrow SegmentVoxelGrid(<i>voxelgrid</i> , <i>method</i>) ;

Algorithm 1: The Dense Data Segmentation Pipeline, With Ground Extraction

3) *Base-Of Method*: In order to test the benefit of using the ground as a separator between objects, a technique which does not rely of the extraction of a ground surface is also defined. The algorithm considers voxels to be either flat or non-flat depending on vertical variance. Flat voxels are grouped together, as are non-flat voxels. Dissimilar voxels are grouped only if the non-flat voxel is below the flat voxel. This last criteria is based on the idea that sections of an object are generally stacked on top of one another because of the influence of gravity, hence some voxels are the *base of* other voxels from the ground up. A typical example observed in the data is the roof of a car, which may be disconnected from to the rest of the car’s body without the ‘base-of’ relationship. In this case, flat voxels forming the roof of the car are connected and non-flat voxels forming the body of the car are also connected, resulting in two partitions. Applying the base-of relationship, the body of the car is interpreted as the base of its roof and the full car is connected into a single segment.

4) *Base-Of With Ground Method*: Ground segmentation is performed and then the Base-Of method is applied to the remaining non-ground voxels.

C. Segmentation for Sparse Data

Two complementary segmentation methods for sparse data are presented; Gaussian Process Incremental Sample Consensus (GP-INSAC) and Mesh Based Segmentation. These methods provide a sparse version of ExtractGround, followed by the use of the Cluster-All approach from Section III-B. The GP-INSAC method is designed to operate on arbitrary 3D point clouds in a common cartesian reference frame. This provides the flexibility to process any source of 3D data, including multiple 3D data sources that have been fused in a common frame. By leveraging the sensor scanning pattern, the Mesh Based method is optimised for 3D point cloud data in a single sensor frame. This provides additional speed or accuracy for particular sensor types.

1) *Gaussian Process Incremental Sample Consensus (GP-INSAC)*: The Gaussian Process Incremental Sample Consensus (GP-INSAC) algorithm is an iterative approach to probabilistic, continuous ground surface estimation, for sparse 3D data sets that are cluttered by non-ground objects. The use of Gaussian Process (GP) methods to model sparse terrain data was explored in [17]. These methods have three properties that are useful for segmentation: (1) they operate on sparse data, (2) they are probabilistic, so decision boundaries for segmentation can be specified rigorously, (3) they are continuous, avoiding some of the grid constraints in the dense methods. However, GP methods typically assume that most of the data pertain to the terrain surface and not to objects or clutter; i.e. they assume there are few outliers. Here, the problem is re-formulated as one of model based outlier rejection, where inliers are points that belong to the ground surface and outliers belong to cluttered non-surface objects, that will ultimately be segmented. The GP-INSAC algorithm maintains the properties of GP terrain modeling techniques and endows them with an outlier rejection capability.

A common approach to outlier rejection is the Random Sample Consensus (RANSAC) algorithm [12]. As the complexity of the model increases, so does the number of hypothetical inliers required to specify it, causing the computational performance of RANSAC to decrease. For complex models including GPs, an alternate approach is presented, called Incremental Sample Consensus. Although motivated by the cases where RANSAC is not practical, INSAC is not a variant of RANSAC as in [12]. Deterministic iterations are performed to progressively fit the model from a single seed of high probability inliers, rather than iterating solutions over randomly selected seeds.

The INSAC method is specified by Algorithm 2. Starting with a set of data and an a-priori seed subset of high confidence inliers, the INSAC algorithm fits a model to the seed, then evaluates this for the remaining data points (similar to the first iteration of RANSAC). All of the non-inlier points are compared with this model (using Eval from Algorithm 2). INSAC uses probabilistic models that estimate the uncertainty of their predictions, leading to two thresholds: t_{model} specifies how certain the model must be for in/outlier determination to proceed. Subsequently, t_{data} specifies the

```

Input      :  $data, modelType, i_{seed}$ 
Output     :  $i, o, u, model$ 
Parameters:  $t_{data}, t_{model}$ 
1  $i = o = u = \{\}$ ;
2  $i_{new} = i_{seed}$ ;
3 while  $size(i_{new}) > 0$  do
4    $i = i \cup i_{new}$ ;
5    $model = Fit(modelType, i)$ ;
6    $test = data - i$ ;
7    $\{i_{new}, o_{new}, u_{new}\} = Eval(model, test, t_{data}, t_{model})$ ;
8    $o = o \cup o_{new}$ ;
9    $u = u \cup u_{new}$ ;
10 end

```

Algorithm 2: The Incremental Sample Consensus (INSAC) Algorithm. For brevity, i, o, u and t represent inliers, outliers, unknown and threshold respectively.

normalised proximity of a datum (x) to the model prediction (μ_{model}), required for the datum to be considered an inlier. This is done using a variant of the Mahalanobis distance to normalise the measure, given estimates of the noise in the data and in the model ($\sigma_{data}, \sigma_{model}$, respectively). The two rules are expressed by:

$$\sigma_{model} < t_{model} \quad \text{and} \quad \frac{x - \mu_{model}}{\sqrt{\sigma_x^2 + \sigma_{model}^2}} < t_{data} \quad (1)$$

If the first inequality fails, a point is classified unknown. Points that pass the first inequality are classified inliers if they also pass the second inequality, otherwise they are outliers. Starting from the seed, inliers are accumulated per iteration. This allows INSAC to ‘search’ the data to find inliers, without allowing unknown points to corrupt the model. Iterations are performed until no more inliers are found. The process combines both extrapolation and interpolation of the model, but only in regions where the certainty is sufficiently high. This can be seen in the sequence of iterations of GP-INSAC in Figure 2. The first iteration extrapolates but misses a point because the data uncertainty is too large. By the third iteration, it has captured this point using interpolation, once the model/data agreement is more likely. Like RANSAC, this method can be used with any core model, however the justification to do so is strongest for complex probabilistic models such as GPs.

The customisation of the INSAC algorithm for terrain estimation using GPs is given in Algorithm 3. The algorithm comprises four key steps; data compression, seed calculation, INSAC and data decompression. Figure 2 shows three iterations of the basic algorithm for simulated 2D data, to illustrate the process, not including compression.

```

Input      :  $x = \{x_i, y_i, z_i\}, i = [0, N]$ ;
Output     :  $i, o, u, model$ 
Parameters:  $t_{data}, t_{model}, GP, r, d, R_s, B_s$ 
1  $x_{gm} = GridMeanCompress(x, r)$ ;
2  $x_{dgm} = Decimate(x_{gm}, d)$ ;
3  $s_{dgm} = Seed(x_{dgm}, R_s, B_s)$ ;
4  $\{i, o, gp_{dgm}\} = INSAC(GP, s_{dgm}, t_{data}, t_{model})$ ;
5  $\{i_{gm}, o_{gm}, u_{gm}\} = Eval(gp_{dgm}, x_{gm}, t_{data}, t_{model})$ ;
6  $\{i, o, u\} = GridMeanDecompress(x, i_{gm}, o_{gm}, u_{gm})$ ;
7  $model = gp_{dgm}$ ;

```

Algorithm 3: The Gaussian Process INSAC (GP-INSAC) Algorithm for Terrain Estimation, with optional Data Compression. i, o, u and t represent inliers, outliers, unknown and threshold respectively.

The ability of GP models to handle sparse data allows an optional step of compressing the data, to decrease the

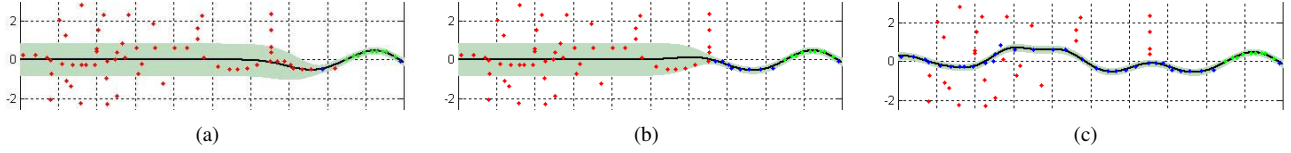


Fig. 2. The GP-INSAC method from Algorithm 3 is run on simulated 2D data. A ground seed is chosen manually, shown in green. The output after the first iteration is shown in (a), after three iterations in (b) and the 16th and final iteration in (c)

computation time. Compression is performed in two stages in lines 1 and 2 of Algorithm 3. The data are first assigned to a fixed 3D grid structure with a constant cell size of r metres. In each cell, the contents are represented by their 3D mean. In the second stage, the data are decimated by keeping 1 in every d of the grid means. The first stage compresses the data towards uniform density, avoiding grid quantisation errors by calculating the means. The second stage allows further compression, without requiring larger (less accurate) cell sizes.

Once the optional compression is performed, an initial seed of likely ground points is determined using the application specific *Seed* function. For this study, the points within a fixed radius R_s of the sensor that are also below the base height B_s of the sensor are chosen ($|\mathbf{x}| < R_s$ and $x_z < B_s$), assuming this region is locally uncluttered by non-ground objects. INSAC is then performed as per Algorithm 2, on the decimated grid means. This classifies the decimated grid mean data into the three classes; inliers, outliers or unknown and provides the GP model representing the continuous ground surface according to the inliers.

The data are then decompressed in lines 5 and 6 of Algorithm 3. The GP model (from the decimated means) is used to classify all of the un-decimated means, using the same function from the INSAC method in line 7 of Algorithm 2 and Equation III-C.1. Finally, the class of the grid means is applied to the full input data by cell correspondence, using *GridMeanDecompress*. The output is the full classification of the original data, as inliers (belonging to the ground), outliers (belonging to an object) or unknown (could not be classified with high certainty).

For sparse segmentation, the ground data produced by GP-INSAC in Algorithm 3 are considered as one partition. The non-ground data are then processed by *SegmentVoxelGrid* with the Cluster-All method from Section III-B.2 to produce the remaining non-ground partitions. Unknown points remain classified as such.

In Section V, the performance of the algorithm is demonstrated with different parameter values and optimal parameter choices are given by comparison with hand partitioned data.

2) *Mesh Based Segmentation*: The Mesh Based Segmentation algorithm involves three main steps: (1) construction of a terrain mesh from a range image; (2) extraction of the ground points based on the computation of a gradient field in the terrain mesh; (3) clustering of the non-ground points using the Cluster-All method.

The generation of a mesh from a range image follows the approach in [9], which exploits the raster scan arrangement for fast topology definition (around 10 ms per scan). An example of the resulting mesh is shown in Fig. 3(a). With

sparse data, such a mesh creates a point-to-point connectivity which could not be captured with a constant resolution grid. As a consequence the ground partition can be grown from a seed region (here, the origin of the scan) through the connected topology.

Once the terrain mesh is built, the segmenter extracts the ground (function *ExtractGround* in algorithm 1) by computing a gradient field in the mesh. For each node (i.e. laser return), the gradient of every incoming edge is first evaluated. The gradient value for the node is chosen as the one with the maximum norm. The four links around a given node are identified as: {UP, DOWN, LEFT, RIGHT}, with DOWN pointing toward the origin of the scan. To compute the gradient on the DOWN edge, for instance, the algorithm traverses the mesh from one node to the following in the DOWN direction until a distance of *mingradist* is covered. The gradient is then obtained as the absolute difference of the height of the starting and ending node divided by the distance between them. If a *mingradist* length is not covered in a given direction, the gradient is disregarded. Enforcing a minimum gradient support length allows noise to be averaged out: as can be seen in Fig. 3(a), the nodes nearer to the centre of the scan are nearer to each other, which generates noisy gradient estimates if consecutive nodes are used to calculate the gradients (since the noise in their height values is of the same magnitude as the length of the links connecting them).

Once the gradient field is computed, the ground partition is obtained by growing a cluster of ground nodes from the closest to the furthest raster line. In the closest raster line (the inner most ring in Fig. 3(a)), the label GROUND is assigned to the longest sequence of nodes s_g with gradients below *maxgrad*. Additionally, sequences of nodes s_i from the inner ring with gradients below the threshold *maxgrad* are also marked GROUND if, given that n_i and n_g are the closest nodes in s_i and s_g , respectively, their height is within *maxdh*. For the other raster lines, a node is marked as GROUND if its gradient value is below *maxgrad*, and it has at least one of its direct neighbours already identified as GROUND; whether this neighbour is in the same raster line or in the previous one. This last requirement encodes the iterative growing of the ground partition and avoids non-ground flat partitions (such as the roof of a car) to be mistaken as part of the ground. This propagation process assumes that the ground can be observed around the sensor; more specifically, it assumes that at least part of the raster line nearest the sensor falls on the ground, and the corresponding set of nodes form the longest flat sequence. The propagation of the GROUND label is performed in both directions in each scan line (i.e. each scan line is traversed

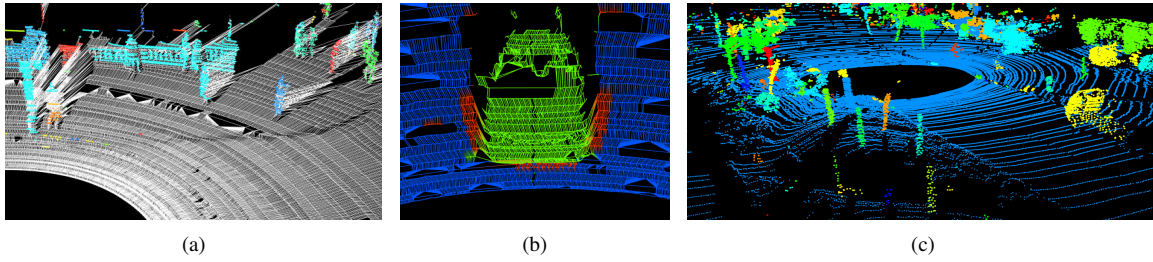


Fig. 3. (a) The mesh built from the range image; points (nodes) identified as belonging to the ground are in white; other colours indicate off the ground segments. (b) An example of transition detection around a car in the terrain mesh: ground points are in blue, non ground points in green, and transition points in red. (c) An example of full segmentation obtained with the combination {Mesh Based segmenter, Cluster-All}. One colour corresponds to one segment.

twice) since intercepting objects may stop the propagation. The extraction of the ground is illustrated in Fig. 3(c).

The last step in the extraction of the ground is the identification of the transitions between the ground and the objects above. The need for transition detection is developed in [4] (Fig. 5). Its effect is illustrated in Fig. 3(b). Transitions are detected by maintaining a buffer of consecutive GROUND node heights (up to ten values are buffered in our implementation). This buffer is slid along each raster line first, and then along each radial line, while GROUND node heights are added in a First In First Out fashion. The buffer is emptied when starting the processing of the next line. A node is marked as TRANSITION if it does not belong to the ground based on its gradient but its height is within $maxdh$ of the buffer mean height. The buffer is slid twice on each scan and radial line; once in each direction along the line in order to identify the transitions on all sides of an object. As illustrated in Fig. 3(b), transition detection allows a tighter segmentation of objects which is essential in cluttered areas.

Once the ground is extracted, the NON-GROUND points are fed to a voxel grid and a Cluster-All segmentation is applied. Note that the points identified as TRANSITION are not passed to the 3D segmenter since this allows a tighter segmentation of objects. This completes the segmentation process as implemented by the Mesh Based Segmenter. Its output is illustrated in Fig. 3(c). In the experiments (Sec. V-B), the three parameters $mingradist$, $maxdh$ and $maxgrad$ are optimised based on hand-labeled segmentations.

IV. METRIC FOR SEGMENTATION EVALUATION

A metric is proposed to quantify the agreement between two segmentations of the same set of data. This can be used to quantify the performance of different segmentation algorithms, by comparison to a hand segmented scene. The general concept of the metric is illustrated in Fig. 4. The tree marked B is the manual segmentation and the tree marked A is an example of flawed segmentation. The largest segment of the voxels in A that comprises the tree is considered the match, in this case the red area of the tree top, and all other partitions are considered errors. Once a segment has been considered as a match, it will be considered as an error in any subsequent match attempts.

The specific comparison process is as follows. First the partitions of the hand-picked data are sorted from largest to smallest. For each reference partition, each data point is

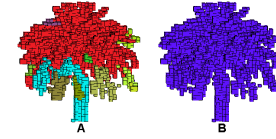


Fig. 4. Example of Segmentation Comparison

matched to the same point in the test segmentation. A list of partition sizes is accumulated based on the partition IDs of the points. The largest partition of test points that correspond to the given hand-picked partition is then considered to be a match. The partition ID that is considered matching is then marked as used and then when any other points with that ID are found they are considered to be in error. Because the comparison is performed in order from the largest partition to the smallest, if a small object is incorrectly grouped to a large object, the smaller object will be considered to be erroneously partitioned and not the larger object. From the points marked as matches and those marked as errors, a percentage match is calculated.

Alternative metrics are also considered. In particular, scoring in terms of voxels instead of points. Since all points in a voxel must have the same partition ID, voxels can be marked as matched or errors when the status of any point within the voxel is determined. Then the voxel match percentage is also calculated. The voxel match percentage tends to be more volatile than the point match percentage. The quality of partitioning of smaller, sparser, more difficult to partition objects is usually better represented by the voxel score due to less domination by ground and wall points. For example, in one of the data sets used here, the ground comprises over 700,000 points of the 1.6 million points in the scan (44%), but only 35,600 voxels of the 143,000 voxels in the segmentation (24%).

V. EXPERIMENTS

This empirical analysis follows the principles laid out by Hoover *et al.* in their reference work on experimental evaluations of segmentation methods for range images [6]. In particular, the parameter space of each algorithm is uniformly sampled to find the combination of parameters providing the best segmentation results with respect to several hand labeled data sets (the use of more sophisticated optimisers is left for future work). Match percentages (relative to the hand segmented data) and computation times are recorded and averaged over the test data sets for each combination of parameters tested. The best results for dense and sparse

data are provided in Tables I and II, respectively. The best results across methods are indicated in bold. The type of implementation used is also indicated. The output of each technique is further illustrated in the video associated with this submission (a longer version of this video is available at: <http://www.acfr.usyd.edu.au/afmr/segmentation/icra11results.wmv>).

A. Dense Data Results

Four hand labeled data sets (with point-wise labels) are used in this first set of experiments: two are formed from a single Riegl scan, one acquired at Drexel University, US, and a second one at the University of Sydney, Australia (Fig. 1); another set is generated by combining vertical scans from a SICK laser with the navigation solution of the mobile platform the sensor is mounted on; and a fourth set is obtained by combining Velodyne scans and navigation data. The four point clouds were acquired in static environments.

1) *Cluster-All Segmentation Method*: For this experiment, the role of voxels size was tested. The two plots in Fig. 5 are the point and voxel scores versus voxel size in centimeters and neighbourhood. The neighbourhood value is the absolute magnitude of the distance two voxels can be away from each other, in terms of voxel grid spaces. For example two voxels that are touching but one grid off in x or y would have a magnitude of 1, and if the voxels were only touching corner to corner that would be a magnitude of 3. The voxel size tests show a peak at 0.2m. In terms of computation times, at a voxel sizes of 0.1m, 0.2m, and 0.4m processing took on average 8.02s, 4.30s, and 3.82s respectively (these times cannot be directly compared to the other tests because a different data structure was used to allow a larger number of voxels to be represented). The peak match percentage occurs with a voxel size of 0.2m. Since a significant time penalty is incurred for smaller voxels and minimal time savings are achieved with larger voxels, the conclusion can be made that 0.2m is optimal based on these tests. The scores reported in Table I correspond to this parameter choice.

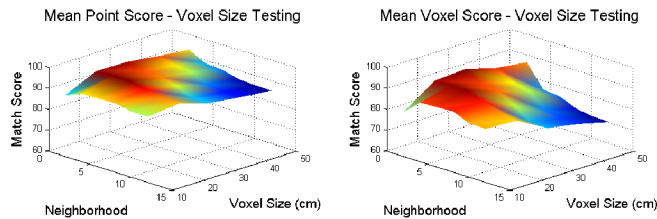


Fig. 5. Cluster-All Segmentation, Scores of Variance Tests and Voxel Size Tests.

A variant of Cluster-All involving a varying neighbourhood size was also tested. It is illustrated in Fig. 7(a). The density of objects and the density of scan points is greater at lower heights above ground due to objects naturally resting on the ground and the corresponding proximity of the sensor. Employing larger neighbourhoods a certain distance above the ground can prevent over-segmentation of high sparse objects while not risking under-segmentation of objects close together on the ground. The corresponding results are reported in the line ‘Cluster-All with Variable Neighbourhood’ of table I. In these tests the neighbourhood was restricted to 3

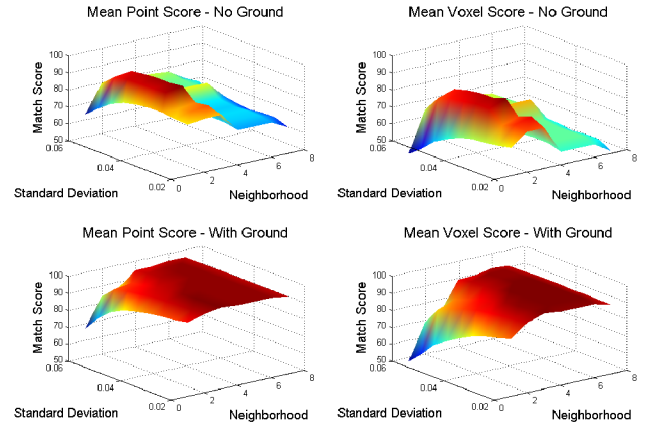


Fig. 6. Base-Of Segmentation, Match Results vs Standard Deviation and 3D Neighbourhood.

for voxels less than 2 meters above the ground and extended to 6 otherwise.

2) *Base-Of Segmentation Method*: For this method two parameters were varied and all tests were run both with and without the ExtractGround operation (Algorithm 1). Fig. 6 shows 3D plots of the average results for the four dense data sets. While Base-Of without ground extraction has the advantage of being almost twice as fast as the ground based methods, it is behind the other techniques in terms of accuracy. This result experimentally confirms the usefulness of explicit ground extraction in 3D segmentation.

B. Sparse Data Results

Four hand labeled Velodyne scans (with point-wise labels) are used for the evaluation of the sparse methods. The results are presented in Table II and were obtained by averaging performance and computation times over the four labeled scans (the same as the dense data results).

1) *Cluster-All Segmentation*: The following three parameters are varied to obtain the best point and voxel scores: *maxvstd*, the maximal vertical standard deviation in a voxel below which this voxel is identified as belonging to the ground in the function ExtractGround; *groundres*, the resolution of the grid used in ExtractGround; *objectres*, the resolution of the grid used in SegmentVoxelGrid. The results are shown in Fig. 7(b). In both cases, the optimal parameter values are 0.3m for *maxvstd*, 0.5m for *groundres* and 0.2m for *objectres*, and correspond to the best scores reported in Table II.

2) *GP-INSAC Segmentation*: The complete GP-INSAC sparse segmentation method has a total of seven parameters, grouped by the stages in the pipeline. INSAC requires t_{data} and t_{model} , the cylindrical seed region requires R_s and B_s , data compression uses r and d , and the final partitioning step is parameterised by the grid resolution. The GP model employs a squared exponential covariance with three parameters: length scale, process and data noise (ls, σ_p, σ_d), which are learnt off-line with a maximum likelihood approach [17], by manually providing segments of ground data. Once learnt, these parameters are fixed for the GP-INSAC algorithm.

The algorithm was run on a range of parameters.

TABLE I DENSE SEGMENTATION MATCH RESULTS

Method	Point Score Range	Voxel Score Range	Computation Times
Cluster-All	97.4	94.3	1.60 - 1.47 sec (C++)
Cluster-All with Variable Neighbourhood	97.7	94.9	1.71 - 1.36 sec (C++)
Base-Of	88.5	79.8	0.76 - 0.70 sec (C++)
Base-Of With Ground	97.2	93.9	1.56 - 1.38 sec (C++)

TABLE II SPARSE SEGMENTATION MATCH RESULTS

Method	Point Score Range	Voxel Score Range	Computation Times
Cluster-All	0.81	0.71	0.42 - 0.42 sec (C++)
GPINSAC	0.89 (on 96%)	0.83	0.17 sec (C++)
Mesh Based	0.92	0.88	0.27 - 0.29 sec (C++)
Convexity Based Segmentation [9]	0.71	0.63	1.76 - 1.69 sec (Python/C++)

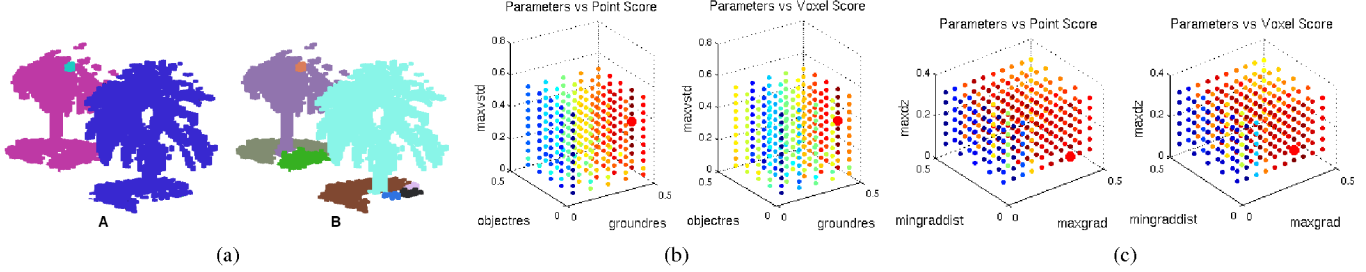


Fig. 7. (a) Segmentation with Fixed Neighbourhood (A) and Variable Neighbourhood (B) showing better segmentation with use of a variable neighbourhood. (b) Point scores (left) and voxel scores (right) obtained when varying the three parameters *maxvstd*, *groundres* and *objectres* in the Cluster-All algorithm. Colours are mapped to scores. The optimum is indicated in each figure by a larger red dot. For the point score, the range of values is: 0.38 to 0.81; for the voxel score, it is: 0.24 to 0.71. (c) Same colour coding as in (b) for the parameters *mingraddist*, *maxdh* and *maxgrad* of the Mesh Based Segmenter. For the point score, the range of values is: 0.56 to 0.92; for the voxel score, it is: 0.47 to 0.88.

The seed cylinder was measured and fixed to $\{R_s=8m, B_s=-1.6m\}$ and the optimal partition resolution for *SegmentVoxelGrid* was fixed to $0.2m$, as determined in Section III-B. Six separate sets of the three GP parameters were learnt, from the four test scans and from two independent training scans. The additional two were included to allow a separate source of training data to be used, allowing the algorithm to be tested on independent test data.

The algorithm was evaluated with the segmentation metric from Section IV and timed on a 2GHZ dual core PC. The results are shown in Figure 8. The parameter sets that produced results with a point score above 80%, a percent classified $> 90\%$ and processing time $< 0.25s$ were selected. The individual parameters that most frequently led to this selection were chosen as optimal. As such, they are likely to be the most stable. This corresponds to the parameter set *Compression* $\{r=0.6m, d=30\}$, *INSAC* $\{t_{model}=0.2m, t_{data}=3sd\}$, *GP* $\{ls=14.01m, \sigma_p=0.88m, \sigma_d=0.060m\}$. Interestingly, the optimal GP parameters were learnt from one of the two independent training samples that was not used in testing. All reported test results are obtained using independent training and test data.

The results using the optimal parameter choice from this test are shown in Table II. The metric indicates an accurate segmentation is produced in the fastest computation time. However, parameters could be chosen to further emphasise accuracy for a larger computational cost. Future work includes testing the algorithms for stability on a larger set of data and it is suspected that GP-INSAC will require a ‘lower’ parametrisation to achieve long term stability. In that case, the mesh segmentation is likely to be closer to real time performance when processing can be done in the sensor frame. The key differentiator of the GP-INSAC algorithm

is that it can process arbitrary 3D data from any source or multiple fused sources.

3) *Mesh Based Segmentation*: The following three parameters are varied to obtain the best point and voxel scores: *mingraddist*, *maxgrad*, and *maxdh* (detailed in Sec. III-C.2). The test results are shown in Fig. 7(c). The best point score is achieved when *mingraddist* is $0.4m$, *maxgrad* is 0.1 and *maxdh* is $0.05m$. The best voxel score is achieved when *mingraddist* is $0.35m$, *maxgrad* is 0.1 and *maxdh* is $0.1m$. The corresponding scores are reported in Table II. Based on the results in Sec. V-B.1, the resolution of the grid used in *SegmentVoxelGrid* was set to $0.2m$.

By generating a mesh of varying resolution in the sensor frame as opposed to relying on a fixed resolution grid for ground model as in the Cluster-All method, the Mesh Based Segmenter is able to better recover the underlying connectivity of objects. Table II shows an improvement in voxel score of up to 24%. Directly representing the sparsity of the data also allows to reduce the size of the data structures deployed which in turn leads to gain in computation times. Table II shows that the Mesh Based Segmenter is about 30% faster than the ‘Cluster-All’ method (both implementations are run on a 3GHz desktop computer). The tendency would be reverted however in the case of dense data since the terrain mesh would become denser while a fixed size grid effectively sparsifies the data to an amount related to its resolution.

4) *Convexity Based Segmentation*: The method proposed by Moosmann *et al.* [9] was implemented and tested for this analysis since the Mesh Based Segmenter relies on the same terrain mesh. The main differences between the two approaches are related to the identification of the ground. Here it is integrated into the segmentation process, while in [9] it is obtained from posterior classification. Also, the reasoning in the mesh is used here for ground extraction

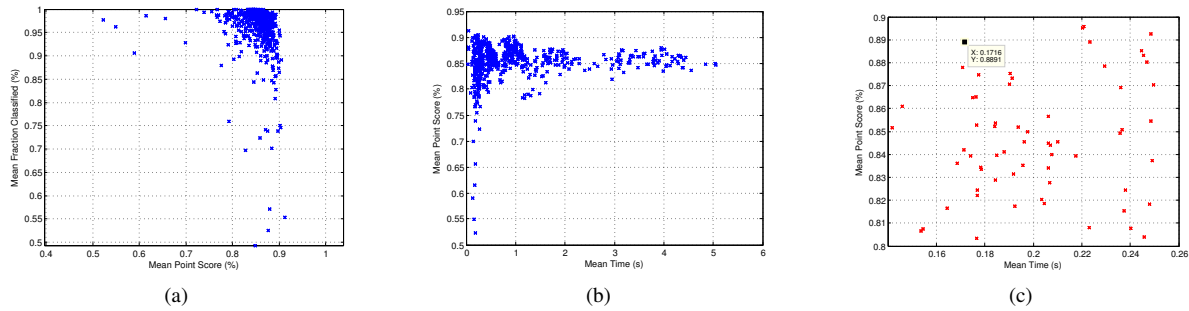


Fig. 8. The results of the GP-INSAC method from Algorithm 3 for different parameter choices, averaged over the four test Velodyne scans. The trade-off between the percentage of points classified vs point score is shown in (a), which indicates a near complete and accurate classification is possible. In (b) the point score and processing time is compared. In (c), only the results with a point score > 0.8 , a percent classified > 0.9 and processing time < 0.25 s seconds are shown. The result from the optimal parameters is highlighted.

only (in the function `ExtractGround`) while it generates the segmentation of the entire 3D space in [9]. Table II shows that the performance of the latter method is lower. As for the other techniques, a range of parameter values was tested and results averaged over the four labeled scans. Following the notations in [9], ϵ_1 was varied from 0 to 45 with a step size of 5, ϵ_2 was varied from 0 to 60 with a step size of 10, and ϵ_3 from 0 to 0.7 with a step size of 0.1. For both point and voxel scores, the optimal values were found to be 40 for ϵ_1 , 50 for ϵ_2 and 0.5 for ϵ_3 . The lower performance is in part due to the limited size of the labeled set and the behaviour of the segmentation metric: for certain combinations of parameters, the segmentation is visually close to the one obtained with the mesh segmenter but the ground is divided into a few main parts which causes a large penalty, since the ground has a dominating weight in both the point and the voxel scores.

VI. CONCLUSION

This study has proposed a set of segmentation methods designed for various densities of 3D point clouds. It first provided empirical evidence of the benefit of ground extraction prior to object segmentation in the context of dense data. The Cluster-All method has achieved the best trade off in terms of simplicity, accuracy and computation times. Its limitations were shown in the context of sparse data and two novel segmentation techniques were proposed for the latter case: the GP-INSAC algorithm for probabilistic ground modeling and for the processing of any 3D point cloud sparse or dense, potentially formed of data accumulated from several sensors; a Mesh Based technique, optimised for the processing of range images. All the algorithms were evaluated on several sets of hand labeled data using two novel metrics.

VII. ACKNOWLEDGEMENTS

This research was undertaken through the Centre for Intelligent Mobile Systems (CIMS), and was funded by BAE Systems as part of an ongoing partnership with the University of Sydney. It was also supported by the ARC Centres of Excellence Programme funded by the Australian Research Council and the NSW State Government. This material is based in part upon work supported by the National Science Foundation under Grant No. 1014634. The authors would like to thank Matthew Johnson-Roberson for useful discussions.

REFERENCES

- [1] O. Khatib B. Siciliano. *Springer handbook of robotics*. Springer, 2008.
- [2] Y. Boykov and G. Funka-Lea. Graph cuts and efficient nd image segmentation. *International Journal of Computer Vision*, 70(2):109–131, 2006.
- [3] J. Diebel and S. Thrun. An application of markov random fields to range sensing. *Advances in neural information processing systems*, 18:291, 2006.
- [4] B. Douillard, J. Underwood, N. Melkumyan, S. Singh, S. Vasudevan, C. Brunner, and A. Quadros. Hybrid elevation maps: 3d surface models for segmentation. In *Proc. of the IEEE/RSJ International Conference on Intelligent Robots and Systems (IROS)*, 2010.
- [5] A. Golovinskiy and T. Funkhouser. Min-cut based segmentation of point clouds. *Princeton University*.
- [6] A. Hoover, G. Jean-Baptiste, X. Jiang, P.J. Flynn, H. Bunke, D.B. Goldgof, K. Bowyer, D.W. Eggert, A. Fitzgibbon, and R.B. Fisher. An experimental comparison of range image segmentation algorithms. *IEEE transactions on pattern analysis and machine intelligence*, 18(7):673–689, 1996.
- [7] T. Malisiewicz and A. Efros. Improving spatial support for objects via multiple segmentations. In *British Machine Vision Conference*, pages 282–289, 2007.
- [8] N. Melkumyan. *Surface-based Synthesis of 3D Maps for outdoor Unstructured Environments*. PhD thesis, University of Sydney, Australian Centre for Field Robotics, 2008.
- [9] F. Moosmann, O. Pink, and C. Stiller. Segmentation of 3D Lidar Data in non-flat Urban Environments using a Local Convexity Criterion. In *IEEE Intelligent Vehicles Symposium*, pages 215–220, 2009.
- [10] D. Huttenlocher P. Felzenszwalb. Efficient graph-based image segmentation. *Int. Journal of Computer Vision*, 59(2):167–181, 2004.
- [11] F. Pauling, M. Bosse, and R. Zlot. Automatic Segmentation of 3D Laser Point Clouds by Ellipsoidal Region Growing. In *Proc. of the Australasian Conference on Robotics & Automation (ACRA)*, 2009.
- [12] Rahul Raguram, Jan-Michael Frahm, and Marc Pollefeys. A comparative analysis of ransac techniques leading to adaptive real-time random sample consensus. In David Forsyth, Philip Torr, and Andrew Zisserman, editors, *Computer Vision ECCV 2008*, volume 5303 of *Lecture Notes in Computer Science*, pages 500–513. Springer Berlin / Heidelberg, 2008.
- [13] J. Schoenberg, A. Nathan, and M. Campbell. Segmentation of dense range information in complex urban scenes. In *Proc. of the IEEE/RSJ International Conference on Intelligent Robots and Systems (IROS)*, 2010. To appear.
- [14] J. Shi and J. Malik. Normalized cuts and image segmentation. *IEEE Transactions on pattern analysis and machine intelligence*, 22(8):888–905, 2000.
- [15] J. Strom, A. Richardson, and E. Olson. Graph-based segmentation of colored 3d laser point clouds. In *Proc. of the IEEE/RSJ International Conference on Intelligent Robots and Systems (IROS)*, 2010. To appear.
- [16] R. Triebel, J. Shin, and R. Siegwart. Segmentation and unsupervised part-based discovery of repetitive objects. In *Proceedings of Robotics: Science and Systems*, Zaragoza, Spain, June 2010.
- [17] S. Vasudevan, F. Ramos, E. Nettleton, and H. Durrant-Whyte. Gaussian process modeling of large-scale terrain. *Journal of Field Robotics*, 26:812840, 2009.
- [18] Z. Wu and R. Leahy. An optimal graph theoretic approach to data clustering: Theory and its application to image segmentation. *IEEE transactions on pattern analysis and machine intelligence*, pages 1101–1113, 1993.
- [19] X. Zhu, H. Zhao, Y. Liu, Y. Zhao, and H. Zha. Segmentation and classification of range image from an intelligent vehicle in urban environment. In *Proc. of the IEEE/RSJ International Conference on Intelligent Robots and Systems (IROS)*, 2010. To appear.